Causal analysis and modeling of unfrozen water in frozen soil based on the coupling of adsorption and capillary action

Xiao Jin[1], Wen Yang[1], Xiaoqing Gao[1], Ye Yu[1], Zhenchao Li[1], Ruiqiang Bai[2]

[1] Key Laboratory of Land Surface Process and Climate Change in Cold and Arid Region, Northwest Institute of Eco-Environment and Resources, Chinese Academy of Sciences, Lanzhou 730000, China.

[2] State Key Laboratory of Frozen Soil Engineering, Northwest Institute of Eco-Environment and Resources, Chinese Academy of Sciences, Lanzhou 730000, China

Corresponding author: Xiaoqing Gao (xqgao@lzb.ac.cn)

Key Points:

- Part unfrozen water in frozen soils is formed by the coupling effects of adsorption effects and capillary action.
- The freezing characteristics of soils with med to low clay content are mainly caused by unfrozen water affected by coupling effects.
- The coupling effects can explain three phenomena of soil freezing characteristic curve with initial water content.

Abstract

Unfrozen water affects the thermal-hydro-mechanical characteristics, microbial activity and freeze-thaw processes in frozen soils. This study found that part of the unfrozen water is formed by the coupling of adsorption and capillary action in soils with mid to low clay content, which is called bound-capillary water and located in nanopores between clay and sand (silt) particles. The nature of the bound-capillary water affects soil freezing characteristics, which varies with the initial water content. The influence of coupling effects arises from the adsorption effects on the clay surface and the capillary action between the clay-sand particles. The adsorption effects (or surface effects) establish an electrical double-layer structure for bound-capillary water. The capillary action (surface tension) forms bound-capillary water in a shape of meniscuses, which significantly increases its content. Here, we established four theoretical models and a parametric model of unfrozen water based on the coupling effects. The basic mathematical expressions of four theoretical models are almost identical to those of 10 existing unfrozen water semi-empirical models, demonstrating that the semi-empirical models are representative of empirical formulas describing the freezing characteristics of the bound-capillary water. A comparison of model results with the measured unfrozen water content of 9 soils verifies that the parametric model is suitable for soils with low to medium clay content.

Introduction

Permafrost is warming at a global scale (Biskaborn et al., 2019). Climate warming, which directly affects the freezing and thawing process, is reducing the area and stability of permafrost, deepening the active layer, and accelerating the decomposition of organic carbon (Panikov et al. al., 2006; Jorgenson et al., 2010; Yang et al., 2010, Hayashi, 2013; Walvoord & Kurylyk, 2016). The ice-unfrozen water phase transition and water migration in the freezing and thawing process lead to the redistribution of water and solutes in the surrounding soil, in turn affecting soil thermal and hydraulic conductivity, microbial activity, frost heaving and thawing settlement, and changes in the mechanical properties of soils (Konrad & McCammon, 1990; Watanabe et al., 2001; Henry, 2007; Wen et al., 2012; Kurylyk & Watanabe, 2013; Walvoord & Kurylyk, 2016; li et al, 2019; Bai et al., 2020). Therefore, modeling of the unfrozen water content based on the freezing-thawing principle is the key to simulating and predicting associated ecological and hydrological changes, and also to calculating the structural strength of frozen soil in cold regions under the background of climate warming (Poutou et al., 2004; Watanabe & Wake, 2009; Iwata et al., 2010; Ge et al., 2011).

As the soil freezes, there is always a residual portion of liquid water, which is called unfrozen water (Dash et al., 1995; Watanabe & Wake, 2009). According to adsorption effects and capillary action, unfrozen water is divided into bound water and capillary water (Chai et al., 2018; Jin et al., 2020b). The bound water is the electrical double-layer solution located on the surface of the clay particles (Saarenketo,

1998; Jin et al., 2020a). Capillary water is formed by the surface tension of soil pores (Mitchell, 1992; Chai et al., 2018). It is interesting that unfrozen water models can be constructed by using individual adsorption effects (Zhang & Lu, 2021), or individual capillary action (Wang et al., 2017; Bai et al., 2018), or a combination of the two (Chai et al., 2018; Zhou et al., 2018). Dash (1989) pointed out that the van der Waals force on the clay surface leads to an exponential relationship between the unfrozen water content and temperature. Xu et al (2010) considered that unfrozen water is a cationic solution formed by clay adsorption. Wang et al. (2017) and Bai et al. (2018) attributed unfrozen water to the capillary action of soil pores. Jin et al. (2020b) believed that adsorption is the main process contributing unfrozen water, and represents a combination of van der Waals force, valence force and electrostatic force, rather than a separate van der Waals force. Zhang and Lu (2021) concluded that bound water dominates the soil freezing characteristics blow 0°C. The applicable temperature range of these unfrozen water models is between the initial freezing point (close to 0°C) and extremely low temperatures (≈ -20°C) of unfrozen water (Bai et al., 2018; Chai et al., 2018; Zhou et al., 2018; Zhang & Lu, 2021). This temperature range obviously includes bound water and capillary water. Some semi-empirical unfrozen water models do not distinguish between bound water and capillary water, and employ the same model parameters within the controlling range of adsorption and capillary action (Anderson & Tice, 1972; Xu et al., 2010; Bai et al., 2018). The freezing point at the transition of bound water and capillary water can be used to quantify the ranges of adsorption effects and capillary action (Chai et al., 2018, Jin et al., 2020b). However, there are big controversies among all the values of the freezing points, which defined as 0, -1.5, -3.2, -6 or -12℃ (Kozlowski, 2007; Tian & Wei, 2014; Chai et al., 2018; Jin et al., 2020b, Zhang & Lu, 2021). In conclusion, the origin of unfrozen water and the freezing point at the transition of bound water and capillary water are uncertain, which hinders the modeling of unfrozen water.

Based on the freezing characteristics of unfrozen water, which is also known as the soil freezing characteristic curve (SFCC), more than 20 theoretical and semi-empirical models have been established (Kurylyk & Watanabe, 2013; Hu et al., 2020). However, most of the theoretical models are too complex to be used either in the field (Wang et al., 2017; Chai et al., 2018; Jin et al., 2020b; Zhang et al., 2021). The problems for the semi-empirical models are the parameters, such as initial water content, residual unfrozen water content, SFCC shape factor, etc., do not have universal expressions although the semi-empirical models have simple expressions and convenient calculations (Michalowski, 1993; Xu et al., 2010; Bai et al., 2018; Zhou et al., 2018, 2020). Consequently, these parameters – which vary widely between soil types – need to be obtained from unfrozen water experiments on the target soils (Xu et al., 2010; Bai et al., 2018; Zhou et al., 2018, 2020). Therefore, in remote permafrost areas with difficult access, only a few unfrozen water models with available parameters such as soil temperature and texture can be used (Anderson & Tice, 1972; Kozlowski, 2007; Jin et al., 2020b). Among these models, the power law models can not simulate the effects of initial water content on SFCC (Kurylyk & Watanabe, 2013; Hu et al., 2020), while the other models which can simulate the

initial water content have a limited range of application (Kozlowski, 2007). In a word, it is urgent that one unfrozen water model needs to be proposed with a wide range of applications, limited input parameters, and accurate output results.

To address the above uncertainties concerning the mechanisms and application of unfrozen-water models, this study established four theoretical models and one parametric model. The theoretical basis of these models is the coupled effects of adsorption and capillary action. The unfrozen water influenced by coupled effects is located in the nanopores formed by the clay and sand particles in soils with low and medium clay content.

Data and Method

Data

Two types of data are used in this paper. The first type comprises microscopic physical quantities of soils (Table 1) (Dobsen et al., 1985), and is used in the electrical double-layer model. The second type comprises measurements of unfrozen water contents of soils with different textures, and is used to validate the results of unfrozen water models. Soil textures are summarized in Table 2, and measured unfrozen water contents are shown in Figures 2. The first data type contains five soil samples with different textures, which cover typical sandy soil, silt and clay. The second data includes 9 types of soils, with specific surface area between 6 - 60.5 m^2g^{-1}, covering soils with low and medium clay content. The categorization of the soil samples is based on the classification system of the U.S. Department of Agriculture (Jin et al., 2020b).

Table 1. Parameters of the soils, electrical double-layer and fitting equations

Soil Samples	Sandy Loam	Loam	Silt Loam	Silt Loam	Silty Clay	Average
Sand (%)	51.51	41.96	30.63	17.16	5.02	
Silt (%)	35.06	49.51	55.89	63.84	47.60	
Clay (%)	13.43	8.53	13.48	19.00	47.38	
σ ($C\cdot cm^{-2}$)	1.520×10^{-5}	1.493×10^{-5}	1.663×10^{-5}	1.658×10^{-5}	1.329×10^{-5}	
n_0 ($mol\cdot cm^{-3}$)	0.535×10^{-5}	0.396×10^{-5}	0.540×10^{-5}	0.577×10^{-5}	0.469×10^{-5}	
A_s ($m^2\cdot g^{-1}$)	52	49	66	119	252	
β	0.945	0.954	0.947	0.945	0.950	0.948
d (Å)	39	45	38.5	37.5	41.5	40.3
δ (Å)	5	5	5	5	5	5
a_1	3.419	4.173	3.396	3.246	3.738	3.59
b_1	0.615	0.604	0.615	0.618	0.610	0.612
a_2	1.384	1.504	1.380	1.354	1.420	1.408
b_2	0.202	0.196	0.202	0.204	0.199	0.201
a_3	12.44	12.42	12.44	12.45	12.43	12.44
b_3	1.668	1.236	1.685	1.799	1.462	1.570
n_δ (mol/L)	2.324	3.137	2.301	2.155	2.652	2.514
n_d (mol/L)	0.160	0.169	0.165	0.163	0.165	0.164
Tw (℃)	-0.0191	-0.0202	-0.0197	-0.0179	-0.019	-0.019

Note: n_0 is the soil solution concentration; σ is the specific charge density; A_s is the Specific surface; The methods of β and d are shown in the literature[38]; The values of β and d represent the

average between 245 and 271 K; d is the thickness of diffusion-layer; δ is the thickness of absorption-layer. a_1, b_1, a_2, b_2, a_3, b_3, β are dimensionless parameters; 1Å = 10^{-10} m = 0.1 nm; T_w is the freezing point of the cationic solution at $x = d$, which is obtained from Eq. (8); n_δ and n_d are cation solution at the starting point ($x = 0$) and the ending point ($x = d$) of diffusion-layer.

Introduction of bound-capillary water

Based on the freezing characteristics of unfrozen water and the actual shapes of clay and sand particles, the spatial distribution of unfrozen water in soils with low-to-medium clay content was assumed (Figure 1). The clay particles have a shape of facets or discs, and the size is much smaller than sand or silt particles. The clay and sand (silt) particles are assumed to form a finite and infinite plane, respectively. The liquid water existed between the clay and sand (or silt) plane. The adsorption effects (surface effects) of the clay particles induce the electrical double-layer structure of the liquid water, and the concentration of the liquid water decreases exponentially with distance from the clay surface (Figure 1). The capillary action induces a meniscus shape of liquid water, and significantly increases the water content (Figure 1b, c). According to the force acting on the electrical double-layer solution, the cation solution can be further divided into the adsorption-layer (also called the Stern layer) and diffusion-layer (also known as the Gouy layer) (Olphen 1964, 1977; Shang et al., 1994). Since the liquid water in the pores between clay and sand contains the properties of bound water and capillary water, we call it as bound-capillary water.

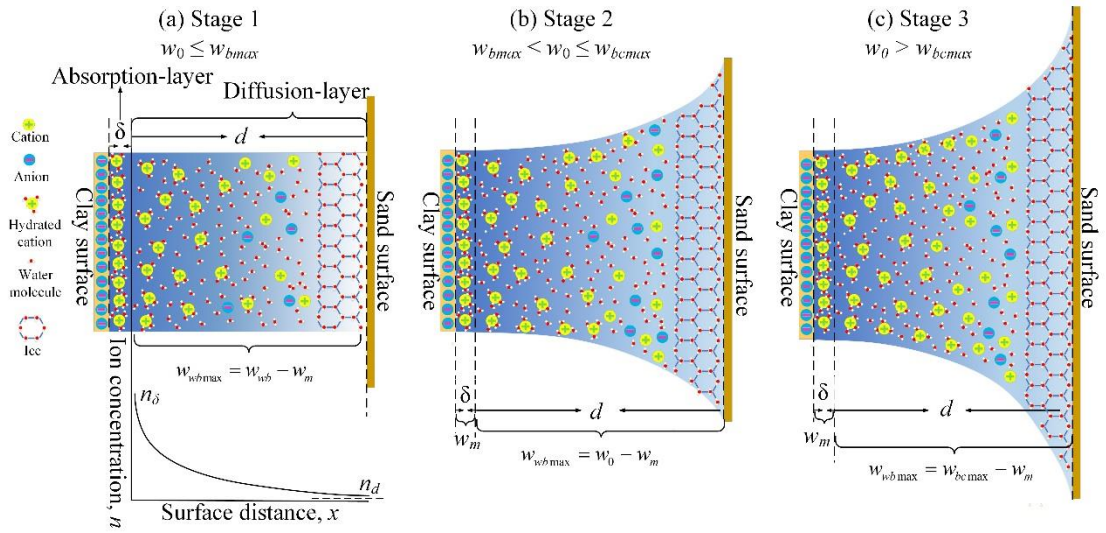

Figure 1 Schematic diagram of the spatial distribution of the ideal bound-capillary water. (w_0 is initial water content; w_{bmax} is the total bound water content; w_{wbmax} is the total weakly bound water content; w_m is the strongly bound water content; δ is the thickness of the adsorption-layer; d is the thickness of the diffusion-layer; x is the surface distance from the interface between the adsorption-layer and the diffusion-layer; n_δ is the cation concentration at $x = 0$; n_d is the cation concentration at $x = d$ close to the edge of the diffusion-layer; the distance between the clay particle and sand (silt) particle is approximately equal to the thickness of the bound water film (≈ 45Å, or 4.5 nm) and the distance is almost constant with w_0 increased)

We define the maximum bound water content (w_{bmax}, equal to the product of the specific surface area (A_S) and the thickness of the electrical double-layer solution) and the maximum bound-capillary water content (w_{bcmax}, equal to the maximum water content between clay and sand particle) to distinguish the characteristics of the bound-capillary water with the initial water content. When $w_0 \le w_{b\max}$ (Figure 1a), the bound-capillary water is mainly affected by adsorption effects, capillary action is negligible, and its content varies linearly with the specific surface area. When $w_{bmax} < w_0 < w_{bcmax}$ (Figure 1b), increasingly important capillary effects induce the meniscus shape of the bound-capillary water, which becomes more obvious closer to the sand surface. The bound-capillary water has the characteristics of both bound water (electrical double-layer structure) and capillary water (meniscus shape). When $w_0 > w_{bcmax}$ (Figure 1c), the shape of the capillary-induced meniscus reaches its maximum curvature, and excess water migrates out of the pores between clay and sand. Based on the variation law and coupling mechanism of capillary-bound water, four theoretical models and a parametric model are established to simulate the freezing characteristics of unfrozen water.

Derivation of unfrozen water models

In this study, the Stern-Gouy electrical double-layer theory is applied to describe the microstructure of the clay surface. Considering that the quantitative calculation of the electrical double-layer model is very complicated, a simple fitting method to describe the cation concentration distribution in the diffusion-layer is established to simplify the derivation and mathematical expression of the unfrozen water model. According to the electrical double-layer theory, the relationship between the surface distance (x) and the cation concentration (n) is as follows (Figure 1) (Olphen 1964, 1977):

$$n(x) = n_0 \left(\frac{1+\beta e^{-x/d}}{1-\beta e^{-x/d}} \right)^{2v/|v|} \tag{1}$$

Here, n_0 is the concentration of the soil solution; v is the average valence of cations; d is defined as the thickness of the diffusion-layer. Actually, d is smaller than the thickness of the fully expanded diffusion-layer of clay particles in a colloidal solution. β is a dimensionless parameter. The values of n_0, d and β are shown in Table 2.

The fitting expressions of relationship between the surface distance (x) and the cation concentration (n) are:

$$x = a_1 n^{-b_1} \tag{2}$$

$$x = \exp(a_2 (\frac{n_d - n}{n - n_\delta})^{-b_2}) \tag{3}$$

$$x = a_3 \exp(-b_3 n) \tag{4}$$

Here, a_1, b_1, a_2, b_2, a_3, b_3 are all fixed parameters of the fitting equations, which represent the characteristics of cation concentration gradient distribution in the diffusion-layer, the results of fitting equations and the values of fixed parameters are shown in the Figure 2 and Table 1, respectively.

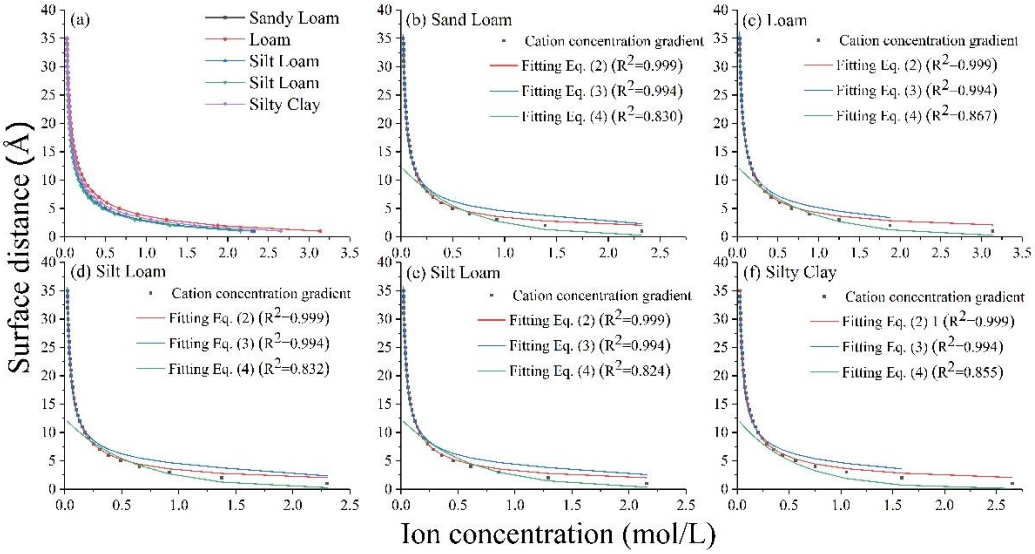

Figure 2 (a) Cation concentration gradient distributions in the diffusion-layer, calculated from electrical double-layer theory (Eq. (1)); (b)-(d) are results of three fitting formulas.

Figure 2 shows the cation concentration gradient calculated by the theoretical formula and three empirical fitting formulas in the diffusion-layer of five soils. The cation concentration gradient decreases exponentially with surface distance. The influence of soil texture on cation concentration gradient is weak (Figure 2(a)): all five kinds of soils, from sandy soil to clay, have almost the same curve. This suggests that the parameters of the fitting equations are weakly independent of the soil texture. Figure 2(b)-(f) compares the fitting equations and the theoretical equations. The results for fitting Eq. (2) and (3) perfectly coincide with the results of the theoretical formula (Eq. (1)), yielding correlation coefficients of 0.999 and 0.994 respectively. Fitting Eq. (4) is a poorer fit than the other two fitting formulas. The respective values of the fitting parameters (a_1, b_1, a_2, b_2, a_3, b_3) in the five soils are very similar, and again are only very weakly dependent on soil texture (Table 1). In summary, the values of the fitting parameters are universal and can describe the cation concentration gradient for a range of soil textures. Since the fitting parameters determine the shape of the curve, these are defined as the shape factors in this study.

Unfrozen water model based on electrical double-layer equation

According to Figure 1, the bound-capillary water between clay and sand particles is divided into three stages. The water content could be expressed as the sum of strongly bound water(w_m) and weakly bound water(w_{wb}):

$$w_u = w_m + w_{wb} \tag{5}$$

The content of strongly bound water is equal to the product of the adsorption-layer thickness (δ) and specific surface area (A_S):

$$w_m = \rho_{bw} A_s \delta \times 10^{-4} \times 100\% \tag{6}$$

where ρ_{bw} is the average density of bound water, which decreases with increasing distance from the clay surface. On average, $\rho_{bw} \approx 1 \mathrm{g/cm^3}$.

The content of unfrozen weakly bound water (w_{wb}) in stage 1 (Figure 1a) is equal to the product of surface distance (x) and specific surface area (A_S):

$$w_{wb} = \rho_{bw} A_s x \times 10^{-4} \times 100\% \tag{7}$$

When $x = d$, w_{wbmax} is the total weakly bound water content, which is equal to the content of the whole diffusion-layer solution.

In Figure 3(a, b), the weakly bound water content (w_{wb}) changes exponentially with the temperature (T), and the concentration (n) of the cation solution in the diffusion-layer also changes exponentially with the surface distance (x). The relationship between solution concentration (n) and its freezing temperature (T) and the relationship between weakly bound water content (w_{wb}) and surface distance (x) are linear. When the relationship between solution concentration (n) and surface distance (x) is known, the relationship between weakly bound water content (w_{wb}) and freezing temperature (T) can then be obtained.

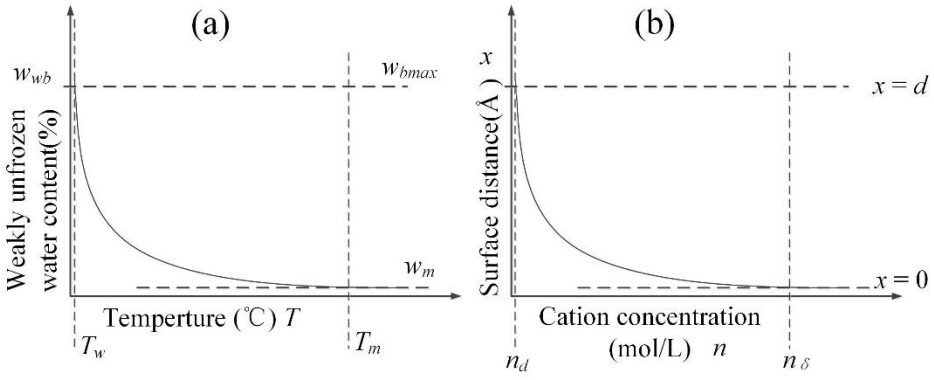

Figure 3(a) The relationship between weakly bound water content and temperature at Stage 1. **(b)** The relationship between cation concentration and surface distance in the diffusion-layer

The linear relationship between cation concentration (n) and freezing temperature (T) is (Banin & Anderson, 1974):

$$n = BT \tag{8}$$

where $B = v/K_f N$, v is the valence of cations in the diffusion-layer, and N is the number of ions ionized by the solute. K_f is a dimensionless coefficient describing the rate of change of freezing point in the soil solution. n_d and n_δ respectively correspond to the

starting point (T_w) and the ending point (T_m) of the curve (Figure 4b). The cation concentrations at these two points can be expressed as:

$$n_d = BT_w \tag{9}$$

$$n_\delta = BT_m \tag{10}$$

The relationship between the surface distance (x) and the freezing temperature (T) of weakly bound water can then be obtained by combining Eqs. (1) and (8):

$$\mathrm{e}^{-x/d} = \frac{1}{\beta}\left(\frac{\sqrt{BT}-\sqrt{n_0}}{\sqrt{BT}+\sqrt{n_0}}\right) \tag{11}$$

Because x is less than d, we use the Taylor expansion of $e^{-x/d}$ and keep only the first-order term:

$$\mathrm{e}^{-x/d} = 1 - x/d \tag{12}$$

Then, from Eqs. (11) and (12):

$$x = -\frac{d}{\beta}\left(\frac{-2\sqrt{n_0}}{\sqrt{BT}+\sqrt{n_0}} + 1 - \beta\right) \tag{13}$$

Since n_0 is very small (Table 1), we have $\sqrt{BT_{wb}}+\sqrt{n_0} \approx \sqrt{BT_{wb}}$. Using this expression, Eq. (13) becomes:

$$x = \frac{2\sqrt{B^{-1}n_0}\,d}{\beta}T^{-0.5} - (1-\beta)\frac{d}{\beta} \tag{14}$$

By eliminating x from the simultaneous Eqs. (7) and (14), the relationship between weakly bound water content and temperature is:

$$w_{wb} = A_s\frac{2\rho_{bw}d10^{-2}\sqrt{B^{-1}n_0}}{\beta}T^{-0.5} - \frac{(1-\beta)d\rho_{bw}10^{-2}}{\beta}A_s \tag{15}$$

Here we define two parameters C_1 and C_{01}:

$$C_1 = \frac{2\rho_{bw}d10^{-2}\sqrt{B^{-1}n_0}}{\beta} \tag{16}$$

$$C_{01} = \frac{(1-\beta)d\rho_{bw}10^{-2}}{\beta} \tag{17}$$

Using C_1 and C_{01}, Eq. (15) is expressed as:

$$w_{wb} = A_sC_1T_{wb}^{-0.5} - C_{01}A_s \tag{18}$$

The expression for total unfrozen water content can then be obtained by bringing the weakly bound water expression (Eq. 5) into Eq. (18):

$$w_u = w_m + A_sC_1T^{-0.5} - A_sC_{01} \tag{19}$$

Next we use the average values (Table 1) of parameters β and d in Eq (17), to obtain $C_{01} = 2.21\rho_{bw}10^{-2}$. The term w_m - A_SC_{01} in Eq. (19) can then be expressed as:

$$w_m - A_S C_{01} = \rho_{bw} A_s 10^{-2}(\delta - 2.21) \tag{20}$$

The adsorption-layer thickness (δ) is not fixed. When the adsorption-layer comprises one layer of hydrated ions ($\delta \approx 2.8$ Å) (Boyarskii et al., 2002), w_m - $A_SC_{01} \approx 0.59A_S\rho_{bw}10^{-2} \approx 0$; or when the adsorption-layer comprises two layers of hydrated ions ($\delta \approx 5$ Å) (Tripathy et al., 2004), w_m - $A_SC_{01} \approx 2.79A_S\rho_{bw}10^{-2} \neq 0$. So when $\delta \approx 2.8$ Å, Eq. (20) can be simplified as:

$$w_u = CT^{-D} \qquad w_0 \le w_{b\max} \tag{21}$$

Where, $C = A_SC_1$, $D = 0.5$.

Unfrozen water models based on the three fitting formulas

The derivation and mathematical expression of the unfrozen water models can be substantially simplified by applying the three fitting formulas (Eqs. 2-4). Combining Eqs. (2) (7) (8), and eliminating the cation concentration (n) and surface distance (x), the relationship between weakly bound water content (w_{wb}) and temperature (T) in the form of power exponent can be obtained:

$$w_{wb} = a_1\rho_{bw}A_s B^{-b_1} \times 10^{-2} T^{-b_1} \tag{22}$$

Similarly, two other expressions can be obtained by combining Eqs. (3) (7) (8) and (4) (7) (8), respectively:

$$w_{wb} = \rho_w A_s \times 10^{-2} \exp(a_2(\frac{T_w - T}{T - T_m})^{-b_2}) \tag{23}$$

$$w_{wb} = \rho_w A_s \times 10^{-2} a_3 \exp(-b_3 BT) \tag{24}$$

The total weakly bound water content (w_{wbmax}) is then the difference between the total bound water content (w_{bmax}) and the strong bound water content (w_m):

$$w_{wb\max} = w_{b\max} - w_m \tag{25}$$

Meanwhile, the total weakly bound water content (w_{wbmax}) can also be expressed as the product of specific surface area (A_S) and diffusion-layer thickness (d):

$$w_{wb\max} = \rho_{bw} A_s d \times 10^{-2} \tag{26}$$

Combining Eqs. (28) and (29), the specific surface area (A_S) can be expressed as the difference between the total bound water content (w_{bmax}) and the strong combined water content (w_m):

$$A_S = \frac{w_{b\max} - w_m}{\rho_{bw} d \times 10^{-2}} \tag{27}$$

Using Eq. (5) and Eq. (27), the unfrozen water models (Eqs. 27-29) can be rearranged as:

$$w_u = w_m + (w_{b\max} - w_m) C_{b1} T^{-b_1} \qquad w_0 \le w_{b\max} \tag{28}$$

$$w_u = w_m + (w_{bmax} - w_m) C_{b2} \exp(a_2 (\frac{T_w - T}{T - T_m})^{-b_2}) \qquad w_0 \le w_{b\max} \tag{29}$$

$$w_u = w_m + (w_{b\max} - w_m) C_{b3} \exp(-b_3 BT) \qquad w_0 \le w_{b\max} \tag{30}$$

Where, $C_{b1} = a_1 (B)^{-b_1} / d$, $C_{b2} = 1/d$, $C_{b3} = a_3 / d$ 。

The input parameters of the five expressions are A_S and T. The other parameters are constant in non-saline soil. The values of a_1, b_1, a_2, b_2, a_3, b_3, d, δ are shown in Table 1; $C_{b1} = 0.327$; $C_{b2} = 0.025$; $C_{b3} = 0.309$; $v \approx 1.8$, $N \approx 2$, $K_f = 7.544$, and $B = 0.1193$. K_f fitted on the measurements and is the only empirical parameter in the models at $w_0 \le w_{b\max}$.

Unfrozen water parametric model based on the bound-capillary water

The four unfrozen water models (Eqs. 21, 28-30) describe the soil water freezing characteristics of the Stage 1 (Figure 1a). Among the 4 formulas, Eq. (21) is based on the theoretical formula (Eq. 1), but its derivation still requires two approximations. When the temperature is close to 0℃, this approximation will increase the model error. The other 3 equations are based on three fitting equations (Eqs. 2-4), for which the power law equation (Eq. 2) has the highest correlation coefficient and the simplest expression when compared with the other two equations (Extended Data Figure 2). Therefore, the unfrozen water model (Eq. 28) is selected to describe the freezing characteristics of the bound-capillary water of Stage 1, 2 and 3. At Stage 2 (Figure 1b) ($w_{bmax} < w_0 \le w_{bcmax}$), the maximum weak bound water content ($w_{wbmax} = w_0 - w_m$) between pores of clay and sand can be expressed as the difference between initial water content (w_0) and strong bound water content (w_m). Using this relationship and Eq. (28), the unfrozen water formula is:

$$w_u = w_m + (w_0 - w_m) C_{b1} T^{-D} \qquad w_{b\max} < w_0 \le w_{bcmax} \tag{31}$$

The shape factor D changes with the soil texture and initial water content. When $w_{bmax} < w_0 \le w_{bcmax}$, the maximum weak bound water content ($w_{wbmax} = w_{bcmax} - w_m$) can be expressed as the difference between the maximum bound-capillary water content ($\le w_0$) and the strongly bound water content, and the unfrozen water content expression is:

$$w_u = w_m + (w_{bcmax} - w_m) C_{b1} T^{-D} \qquad w_0 > w_{bcmax} \tag{32}$$

The water outside the clay-sand (silt) nanopores will freeze rapidly when the

temperature is slightly lower than 0℃, and in this case the parametric model does not predict the water content outside the nanopores. Combined with Eqs. (28, 31, 32), the expression for the unfrozen water parametric model is as follows:

$$w_u = \begin{cases} w_m + (1.6w_{b\max} - w_m)C_{b1}T^{-D} & w_0 > w_{bcmax} \\ w_m + (w_0 - w_m)C_{b1}T^{-D} & w_{b\max} < w_0 \le w_{bcmax} \\ w_m + A_S C_{b0}T^{-D} & w_0 \le w_{b\max} \end{cases} \tag{33}$$

Using Eq. (27), we have adopted another form of formula (28) because it is more convenient at $w_0 \le w_{bmax}$. The parameter D at three stages also changes with the initial water content. When $w_0 \le w_{bmax}$, adsorption effects dominate unfrozen water, and $D = b_1 = 0.612$ is a constant. When $w_0 > w_{bcmax}$, D is affected by the coupling effects of adsorption and capillary action. In this case the initial water content has little influence on the adsorption effects and could be ignored. Therefore, D only changes with the clay content, and its expression can be obtained by fitting the measured unfrozen water data: $D = b_1+(A_S/120)^2$. When $w_{bmax} < w_0 \le w_{bcmax}$, the meniscus formed by capillary effects changes with the initial water content, so D depends on both w_0 and A_S. The fitting expression is then: $D = b_1+((w_0 - w_{bmax})/0.6w_{bmax})(A_S/120)^2$. In summary, D can be expressed as:

$$D = \begin{cases} 0.612 + (A_S/120)^2 & w_0 > w_{bcmax} \\ 0.612 + (w_0 - w_{b\max})(A_S/120)^2 / 0.6w_{b\max} & w_b < w_0 \le w_{bcmax} \\ 0.612 & w_0 \le w_{b\max} \end{cases} \tag{34}$$

Here, $w_{bmax} = 0.38A_S$, $w_m = 0.05A_S^{0.9}$, $C_{b0} = a_1\rho_{bw}B^{-b1}10^{-2} = 0.132$, $C_{b1} = a_1B^{-D}d^{-1} = 0.092 \times 0.12^{-D}$. where C_{b1} changes with w_0 and A_S. $w_{bcmax} \approx 1.6w_{bmax}$ and is obtained by fitting measured data. Eq. (33) is the final unfrozen water parametric model, which only includes three input parameters: initial water content, specific surface area, and temperature. Since the influence of overlapping electrical double-layers is not considered, the parametric model is not suitable for soils with high clay content.

This simple method can be used to calculate unfrozen water content based on the characteristics of the bound-capillary water when the initial water content is unknown. Assuming that the normal water content of soil is 20-40%, the w_0 of sand or silt is usually greater than its maximum content of bound-capillary water (w_{bcmax}), so Eq. (32) can be used to calculate the unfrozen water content:

$$w_u = w_m + (1.6w_{b\max} - w_m) \cdot 0.092 \cdot 0.12^D T^{-D} \qquad w_0 > w_{bcmax} \tag{35}$$

where $D = b_1+(A_S/120)^2$.

The water content of soils with a medium clay content usually closes to w_{bmax} and w_{bcmax}, so we assume that its w_0 is equal to the average of w_{bmax} and w_{bcmax}, and then its unfrozen water content can be calculated by Eq. (31):

$$w_u = w_m + (1.3w_{b\max} - w_m)0.092 \cdot 0.12^D T^{-D} \qquad w_{b\max} < w_0 \le w_{bcmax} \tag{36}$$

where $D = 0.612 + 0.5(A_S/120)^2$

Although this simple method will reduce the accuracy of the model results, it

will increase the scope of application of the parametric model. In addition, many methods have been established to predict the specific surface area of soil based on the soil particle size distribution (Sepaskhah & Tafteh, 2013). Therefore, the unfrozen water content can be obtained only by the soil temperature and soil particle size distribution. This simple method is especially suitable for sparsely populated areas such as the Arctic and Qinghai-Tibet Plateau, where the measurements of initial water content and other physical quantities are very difficult.

Results of unfrozen water parametric model

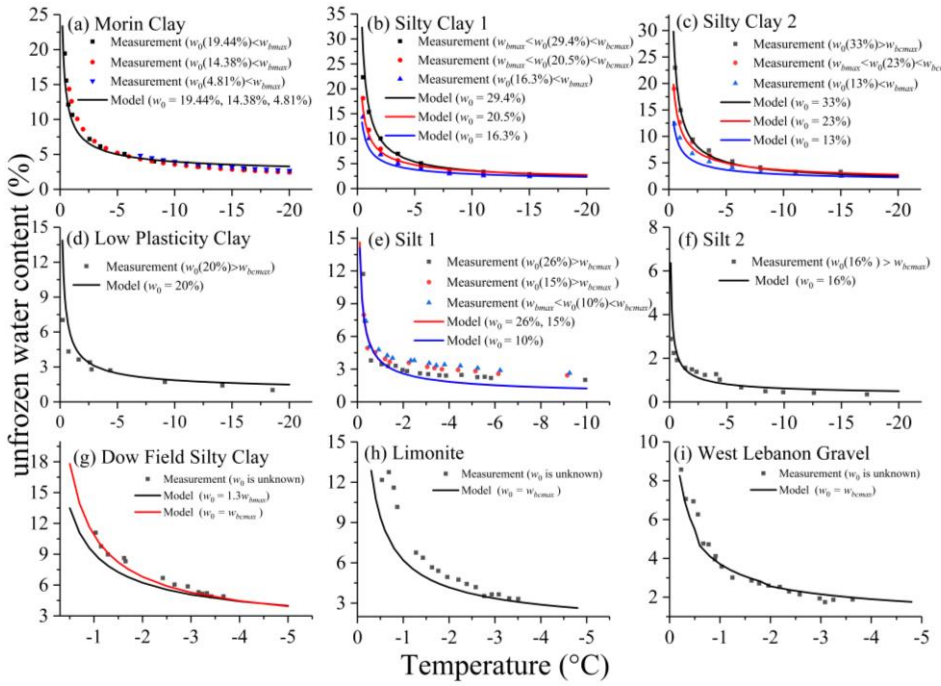

Figure 4 Comparison between the parametric model and the measured unfrozen water content (Physical parameters of soils are shown in the Table2; the root mean square errors (RMSE) of the parametric model are shown in the Table5).

Figure 4 shows the measured unfrozen water content of 9 soils and compares these with the two methods based on the unfrozen water parameter model established in this study. The first is the ordinary method of parameter model (Eq. 33), and the input parameters include temperature, initial water content and specific surface area. The second is the simple method of parameter model (Eqs. 35, 36), and the input parameters only include temperature and specific surface area. Figure 4(a)-(f) shows the results of the ordinary method and Figure 4(g)-(i) shows the results of the simple method. When $w_0 \leq w_{bmax}$, the parametric model ignores the influence of w_0 on adsorption effects. So regardless of how w_0 changes, the model only gives a curve and the model results are consistent with the three measured SFCCs for different w_0 (Figure 4(a)). When $w_{bmax} < w_0 \leq w_{bcmax}$, the w_0 mainly affects the SFCCs by changing the meniscus shape of the bound-capillary water. Figures 4 (b) and (c) show that the model results of three w_0 are in quite close agreement with the measured SFCCs,

indicating that the parametric model simulates the influence of w_0 on SFCCs by capillary action. When $w_0 > w_{bcmax}$, the meniscus curvature of the bound-capillary water reaches its maximum. The w_0 affects SFCC by changing the soil solution concentration and the parametric model ignores this influence. For the low plasticity clay (Figure 4(d)) and Silt 2 (Figure 4(f)), the model results are in close agreement with the measured SFCCs in the range 0 to -20℃, but the model results for Silt 1 (Figure 4(e)) are poor, especially when w_0 is 10%, which shows that the influence of w_0 through the adsorption effects could be considered at $w_0 > w_{bcmax}$.

Figure 4(g-i) shows the results of the simple method in the case of unknown w_0. The model results for Limonite and West Lebanon Gravel, with their small specific surface areas, are consistent with the measured SFCCs; this shows that the simple method is suitable for silt and sand. When the temperature is lower than -2℃, the model results for Dow Field Silty Clay are consistent with the measured SFCC (black curve in Figure 4(g)), but the model results are obviously lower than the measured unfrozen water content in the range of 0 to -2℃. However, the model results (red curve in figure 4(g)) after replacing w_0 with w_{bcmax} agree well with the measured data. Therefore, it is best to apply a parametric model including w_0 for soils with medium clay content. The semi-empirical models with universal expression in empirical parameters can be divided into two categories. The one in the form of power law can not simulate the impact of initial water content on SFCCs, while the other which can simulate this impact is only suitable for the clay soil with temperature between 0 and -6℃. The parametric model is suitable for medium and low clay content soils (clay $\lessapprox$ 24%, $A_S \lessapprox 60.5$ m^2/g). Accurate results proved that there is capillary-bound water on the coupling effects by adsorption and capillary action in the nanopores formed by clay and sand particles, and the freezing characteristics of soils with medium and low clay content are mainly caused by the capillary-bound water.

Table 2 Soil types and physical parameters

Type of soils	A_S (m^2g^{-1})	w_0 (%)	w_p (%)	T_f (℃)	w_{bmax} (%)	w_{bcmax} (%)	References
Morin Clay	60.5	19.44, 14.3, 4.81	22.8	0.43, 0.77, 8.15	22.99	36.78	Xu et al (1985)
Silty Clay 1	52	29.4, 20.5, 16.3	12.5	0.04, 0.09, 0.14	19.76	31.61	Wen et al (2012)
Silty Clay 2	50	33, 23, 13	17.94	0.08, 0.17, 0.53	19.00	30.4	Chai et al (2018)
Xian Loess	39	25, 20, 15, 10, 5			14.82	23.71	Tang et al (2018)
Low Plasticity Clay	22.63	20	22.5	0.39	8.59	13.75	Ma et al (2015)
Silt1	16.6	26，15，10	15.6	0.09	6.31	10.09	Zhou et al (2020)

Silt2	6.22	16	19.8	0.44	2.36	3.78	Ma et al (2015)
Dow Field Silty Clay	50				19	30.4	Anderson & Tice (1972)
Limonite	26				9.88	15.8	Anderson & Tice (1972)
West Lebanon Gravel	18				6.84	10.94	Anderson & Tice (1972)

Note: A_S is the specific surface area. A_S of Silty Clay 1 and Silty Clay 2 are calculated by a fractal dimension method which requires the particle size distribution (Sepaskhah & Tafteh, 2013). A_S of the remaining soils were measured. W_p is the measured plastic limit. $T_f = -0.0729 w_P^{2.462} w_0$, is the freezing point of water (Kozlowski, 2007). w_{bmax} and w_{bcmax} are the maximum bound water content and the maximum content of bound-capillary water.

Discussion

Causal analysis of freezing characteristics with initial water content

The influence of the initial water content on the soil freezing characteristic curve (SFCC) is very complicated. During the experiments, two phenomena, which the initial water content has effect and does not have effect on the soil freezing characteristic curve, appears at the same time, and no models so far can explain this (Watanabe & Wake, 2009; Wen et al., 2012; Chai et al., 2018; Zhou et al., 2020). We found that the variation of SFCC with initial water content could be summarized into three phenomena, and the coupling effects can reasonably explain the causes of the three phenomena.

According to the relationship among the initial water content (w_0), maximum bound water content (w_{bmax}) and maximum bound-capillary water content (w_{bcmax}), three types of experimental phenomena are categorized (Figure 4). (1) When $w_0 \leq w_{bmax}$, the w_0 slightly affects the measured SFCCs, and the SFCCs with low w_0 are slightly higher than those with high w_0 (Figure 4a, referred as Phenomenon 1 hereafter). At this stage, the unfrozen water only contains cationic solution. the exponential distribution of cation concentration in diffusion-layer is the main reason causing the exponential change of unfrozen water content with soil temperatures. The higher the solution concentration is, the lower the freezing point will be. Because the negative charge density on the clay surface is constant, the variation of the w_0 will change the cation concentration gradient distribution. As the w_0 decreases, the cationic solution in the diffusion-layer reduced in content. In addition, the concentration of the cation solution is exponentially distributed and most of the cation solution is distrusted on the surface of the clay. As a result, a slight increase of cation concentration can balance the decrease in the number of cations caused by the decrease of the w_0. When the soil freezes, the cation concentration gradient distribution with low w_0 is slightly higher than that with high w_0. Therefore, the SFCCs with low w_0 slightly lay above the SFCCs with high w_0 in the graph (Figure 4a).

When $w_{bmax} < w_0 \leq w_{bcmax}$, the w_0 mainly affects the bound-capillary water through capillary action (Figure 4b, c). When soil temperature is below 0°C, the bound-capillary water with low cation concentration begins to freeze on the surface of the sand (silt). Because the solution has a meniscus shape, the content of unfrozen solution at high w_0 is higher than that at low w_0. When the temperature is extremely low (≈ -20°C), the bound-capillary water with high cation concentration is mainly located on the clay surface. Since the meniscus curvature on the surface of the clay is close to zero, the unfrozen content of bound-capillary water with different w_0 is the same. It is the meniscus shape which makes the SFCCs indicate the varying characteristics with different w_0 (Phenomenon 2).

When $w_0 > w_{bcmax}$, the content of bound-capillary water and the curvature of the meniscus reach their maxima. An increase in w_0 can reduce the concentration of the water solution outside of the clay-sand nanopores, which is equal to the soil solution concentration (n_0) at the outermost periphery of the electrical double-layer. The decrease of the soil solution concentration contributes to a slight decrease in the cation concentration gradient distribution (Jin et al., 2020b). When the soil freezes, the SFCCs with low w_0 are situated slightly higher than those with high w_0 (Figure 4e, Phenomenon 3). The Occurrence of phenomena 1, 2, 3 and their transform from one phenomenon to another highly depend on the dynamic relationship between clay content and water content in the soil. Phenomena 1 and 2 mainly occur in soil with medium clay content (Xu et al., 1985; Wen et al., 2012; Chai et al., 2018). Phenomenon 3 is mainly found in silt and sand soil types with low clay content (Watanabe & Wake, 2009; Zhou et al., 2020).

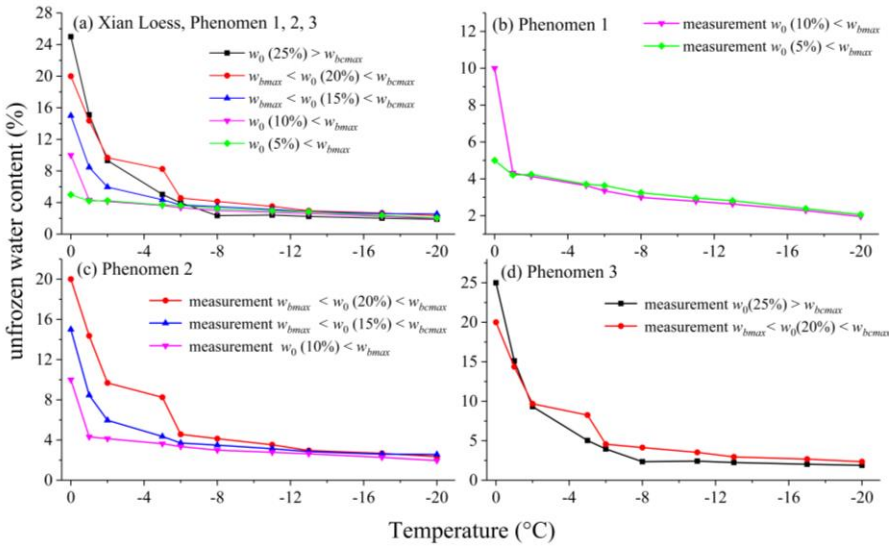

Figure 5 Measured unfrozen water content with different initial water content (Physical parameters of Xian loess are shown in the Table2)

Figure 5 shows the unfrozen water experiment of Xian loess. Phenomena 1, 2 ,3 appear successively with the increase of initial water content. When the w_0 is less than the w_{bmax}, the SFCCs of purplish red and green are completely consistent in the range of -1 to -20°C (Figure 5b), which is consistent with Phenomenon 1. With the increase of w_0, there are obvious differences among SFCCs of blue, red and purplish red

(Figure 5c), which is consistent with Phenomenon 2. When the w_0 continues to increase, the SFCCs of black and red with the w_0 greater than and close to the w_{bcmax} approximately coincide (Figure 5d), which is consistent with phenomenon 3. In general, the unfrozen water experiment of Xian loess supports the existence of bound-capillary water in soils affected by coupling effects.

Comparison of Traditional classification of soil moisture

Traditional view believed that bound water is located on the surface of clay particles, with capillary water or free water beyond the periphery of the bound water (Figure 6) (Chai et al., 2018, Zhang et al., 2021). This assumption is widely used to model unfrozen water content, hydraulic conductivity, permittivity of soils, etc (Wang & Schmugge, 1980; Mironov et al., 2013; Peters, 2013; Chai et al., 2018; Jin et al., 2020b; Zhang et al., 2021). But phenomena 1 and 2 in Figure 4(b), (c) and Figure 5(c) are inconsistent with this traditional view. When $w_0 \leq w_{bmax}$, the measured SFCCs (blue triangle in Figure 4(b), (c)) are almost coincident with the modelled SFCCs (blue curve), and the unfrozen water is bound water. According to the traditional view, when the initial water content increases reach $w_0 > w_{bmax}$, the SFCCs with high w_0 ($w_0 > w_{bmax}$) should extend to 0℃ along the same SFCC as that with low w_0 ($w_0 \leq w_{bmax}$). However, the measurements show that the SFCCs with high w_0 (black and red curves in Figure 4(b), (c)) are above the SFCCs with low w_0 (blue curves). Therefore, phenomena 1 and 2 demonstrate that the traditional view – that the capillary water lies beyond the periphery of the bound water – is unreasonable.

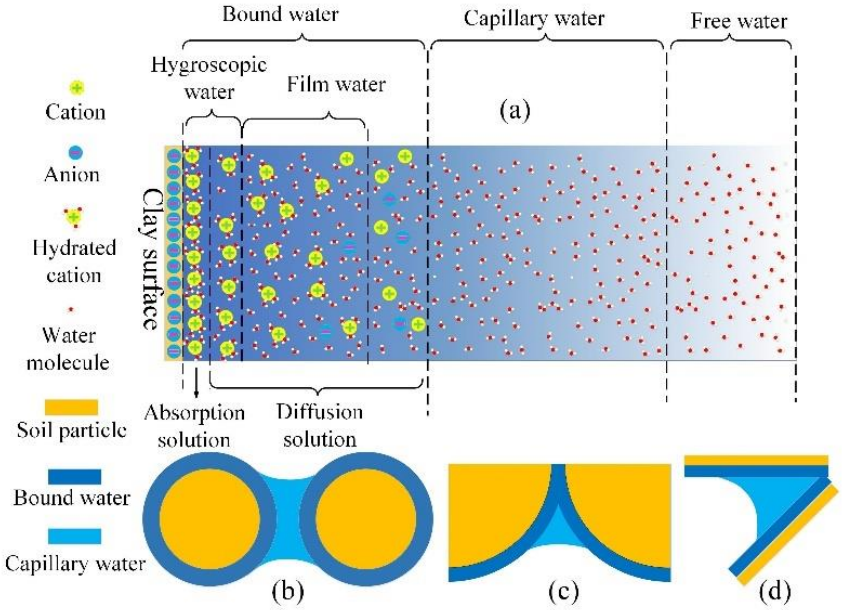

Figure 6 Schematic diagram of traditional soil water distribution (b, c and d are from literature Chai et al (2018), Sheshukov & Nieber (2011), Zhang & Lu (2019), respectively)

The existing soil unfrozen water and dielectric models underestimate the content of bound water (Kozlowski, 2007; Chai et al., 2018; Jin et al., 2020a; Mironov et al., 2013). Taking 19% Morin clay as an example (A_S = 60.5 m^2g^{-1}), assuming that the thickness of the water film is equal to the thickness of the electrical double-layer, we

found that the maximum bound water content (w_{bmax}) is 22.99%, and the maximum bound capillary water content (w_{bcmax}) is 36.78% (Table 2). When $w_0 \leq w_{bmax}$, the results of the unfrozen water model (blue curve in Figure 4a, b, c) based on the electrical double-layer theory for Morin clay, Silty clay 1 and Silty clay 2 are almost completely consistent with the actual measurement in the range of T_w (T_w is slightly less than 0°C) to -20°C. This phenomenon indicates that the freezing point of soil bound water is between T_w and -20°C.

Comparison of semi-empirical and theoretical models

Table 3 Semi-empirical unfrozen water models

No.	Model	Parameters	Reference
1	$w_u = CT^{-D}$	$C = 1.299A_s^{0.552}$ $D = 1.449A_s^{-0.264}$	Anderson & Tice (1972)
2	$w_u = CT^{-D}$	$D = \frac{\ln w_0 - \ln w_m}{\ln T_m - \ln T_f}$ $C = w_0 T_f^{\,D}$	Xu et al (1985) Xu et al (2010)
3	$w_u = CT^{-D}$	$C = \rho_s(1-P)/100\rho_w \exp(0.5519 \times \ln(A_S) + 0.2168)$ $D = \exp(-0.2640 \times \ln(A_S) + 0.3711)$	Kurylyk & Watanabe (2013)
4	$w_u = CT^{-D}$	$C = A_S \rho_w (\frac{-273.15A}{6\pi\rho_i H_f})^{1/3}$ $D = 1/3$	Kurylyk & Watanabe (2013) Hu et al (2020)
5	$w_u = C(T_0 - T')^{-D}$		Zhang et al (2008)
6	$w_u = C\lvert T_f \rvert^D T^{-D}$		Nicolsky et al (2017)
7	$w_u = CT^{-D} + w_m - 0.25C$	$w_m = 5A_S \times 10^{-2}$ $C = 0.0152A_S\sqrt{T_0 - T}$ $D = 0.5$	Jin et al (2020b)
8	$w_u = w_m + (w_0 - w_m)(\frac{T_0 - T'}{T_0 - T_f})^{-D}$		Zhou et al (2018, 2020)
9	$w_u = w_m + (w_0 - w_m)\exp\left[a(\frac{T_f - T}{T - T_m})^b\right]$	$w_m = 0.042A_s + 3$ $a = 3.35$, $b = 0.37$	Kozlowski (2007)
10	$w_u = w_m + (w_0 - w_m)$ $\exp(-a(T - T_f))$		Michalowski (1993) Bai et al (2018)

Note: $T_0 = 273.15$ K, T' is the thermodynamic temperature. For convenience, Table 3 lists the main expressions of unfrozen water models.

Table 3 shows the expressions of unfrozen water semi-empirical models (No.1-10). Some of those models share similar mathematical structures and the same

parameters, so we can simplify and classify these models. According to the relationship between thermodynamic temperature and degrees Celsius, T_0 - T = T, the formula (No.5) can be expressed as w_u=CT^{-D}. When the temperature T changes between 0 and -20 degrees, the average value of the term 0.25C in formula (No.7) is 0.0616A_S, and the expression of term w_m - 0.25C is equal to -0.0116A_S. When A_S < 100, then the expression w_m - 0.25C < 1% and can be omitted. The formula (No.7) can be rewritten as w_u=CT^{-D}. In summary, formulae No.1 to 7 can be expressed as w_u=CT^{-D}.

The freezing point T_f of unfrozen water in ordinary frozen soil is between 0 and -0.3℃[33]. Applying T_0 - T = T and omitting T_f, the formula (No.8) can be expressed as:

$$w_u = w_m + (w_0 - w_m)CT^{-D} \tag{37}$$

where, $C = T_0^{-D}$. Similarly, by omitting T_f, formulae (No.9 and No.10) can be expressed as:

$$w_u = w_m + (w_0 - w_m)\exp\left[a\left(\frac{T}{T_m - T}\right)^b\right] \tag{38}$$

$$w_u = w_m + (w_0 - w_m)\exp(-aT) \tag{39}$$

Through simplification, the ten semi-empirical models are classified into four forms. Similarly, the theoretical models (Eqs. (21) (28) (29) (30)) could be simplified and adjusted. The four theoretical models are expressions of freezing characteristics of electrical double-layer at $w_0 \le w_{bmax}$, so when the $w_0 > w_{bmax}$, w_{bmax} need to be replaced by w_0. The shape factors such as a_1, b_1, a_2, b_2, a_3, b_3 need to be adjusted with the A_S and w_0. In addition, the freezing point T_w (≈-0.019℃) could be omitted in the Eq. (29). The simplified semi-empirical models and theoretical models are shown in Table 4.

Table 4 Unfrozen water theoretical models and semi-empirical models

No.	Semi-empirical models	Theoretical models
1	$w_u = CT^{-D}$	$w_u = CT^{-D}$
2	$w_u = w_m + (w_0 - w_m)CT^{-D}$	$w_u = w_m + (w_0 - w_m)C_{b1}T^{-D}$
3	$w_u = w_m + (w_0 - w_m)\exp\left[a\left(\frac{T}{T_m - T}\right)^b\right]$	$w_u = w_m + (w_0 - w_m)C_{b2}\exp\left[a\left(\frac{T}{T_m - T}\right)^b\right]$
4	$w_u = w_m + (w_0 - w_m)\exp(-aT)$	$w_u = w_m + (w_0 - w_m)C_{b3}\exp(-aBT)$

Note: the semi-empirical model (1-4) is the standard form or the simplified forms of the formula (4.1-4.10) in Table 3; the theoretical models (1–4) are the adjusted Eqs. (21), (28), (29), (30), respectively; Table 4 lists the main expressions of unfrozen water models.

In this study, three fitting equations were established to describe the gradient of the cation concentration in the diffusion-layer. Based on these three fitting equations and the electrical double-layer equation, four theoretical models of unfrozen water were established. The mathematical expressions of the four theoretical models represent the existing 10 semi-empirical models (Table 3), demonstrating that that the

semi-empirical model provides a suitable empirical formula describing the freezing characteristics of the bound-capillary water. The differences between the four types of theoretical models and semi-empirical models lie in the parameters (C_{b1}, C_{b2}, C_{b3}, B in Table 1), which include one or more parameters related to the electrical double-layer (diffusion-layer thickness d, shape factors a_1, b_1, a_2, b_2, a_3, b_3), soil solute parameters (soil solution concentration n_0, solute valence v, and solution ionization number N), and the density of bound water. These parameters are regarded as constants in ordinary soil (non-saline soil). This property significantly simplifies the modeling of unfrozen water, allowing unfrozen water content to be calculated with just the conventional parameters such as specific surface area, temperature, and initial water content. In addition, changes in soil salinity only affect these parameters, and not the mathematical expressions of the unfrozen water models, enabling the power law expressions to be applicable for modeling unfrozen water in saline soils.

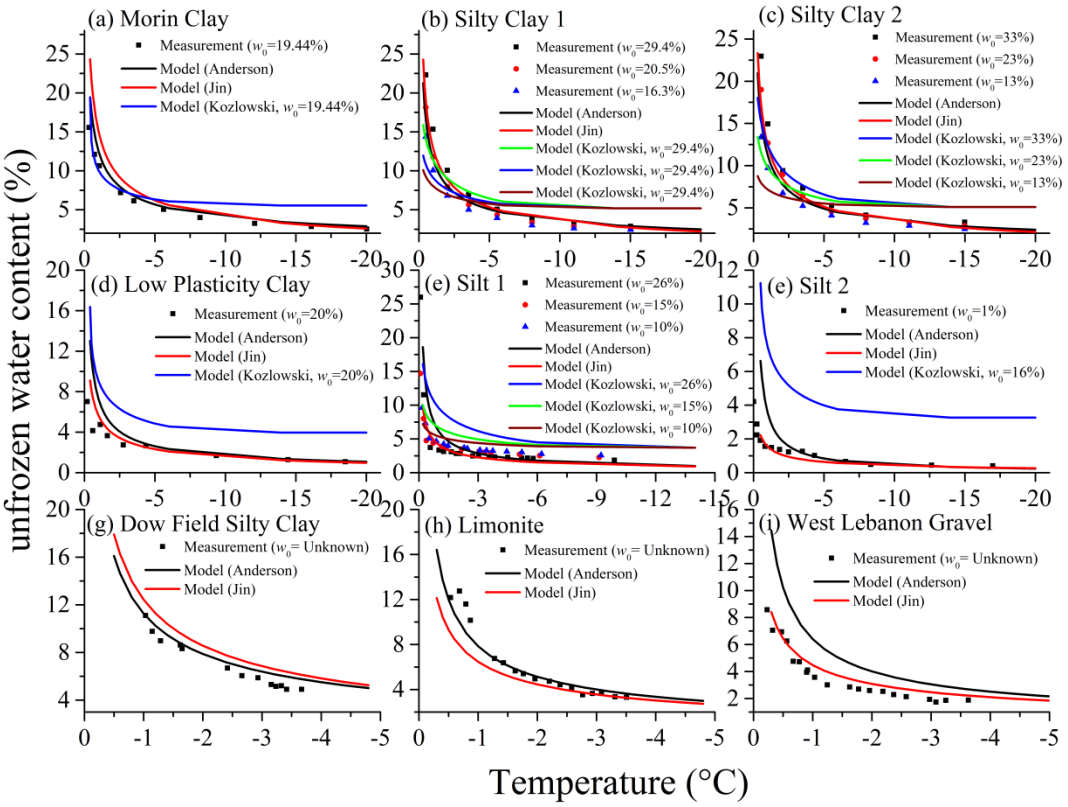

Figure 7 Comparison of the results of three semi-empirical models and the measured unfrozen water content (Physical quantities of soils are shown in Table 2)

Figure 7 shows the results of the three semi-empirical models of Anderson (No.1), Jin (No.7), and Kozlowski (No.9) in Table 3. The parameters of three models have universal expressions. The other semi-empirical models not be used because their expressions are very complex or their parameters need to be fitted by the measured soil freezing characteristic curve. The Anderson and Jin models have good results for 9 soils, but they cannot describe the influence of the initial water content. For soils with low clay content (Low Plasticity Clay, Silt1, Silt2, West Lebanon Gravel), the Jin model is more accurate. The Kozlowski model can describe the effects of initial water content, but it is only suitable for moderate clay content with

the temperature range between 0 and -6 degrees. Combined with RMSEs of models in Table 5, the parametric model proposed in this research has better results and a wider range than semi-empirical models.

Table 5 Root Mean Square Error (RMSE) of unfrozen water models

Type of soils	Initial water content (w_0)	Unfrozen models			
		This study	Anderson	Jin	Kozlowski
Morin Clay	19.44	0.58	1.08	2.48	1.75
	14.3	1.13	0.44	1.14	2.96
	4.81	0.37	0.13	0.12	2.15
Silty Clay 1	29.4	1.50	3.12	2.15	3.80
	20.5	0.92	0.86	0.68	3.22
	16.3	1.13	1.07	1.95	2.63
Silty Clay 2	33	2.58	3.03	2.25	3.06
	23	0.76	1.37	0.61	3.09
	13	0.95	1.10	1.88	2.58
Low Plasticity Clay	20	3.54	11.18	5.26	3.31
Silt1	26	3.42	2.34	3.61	4.57
	15	0.85	5.09	0.92	1.94
	10	1.10	3.01	1.11	1.06
Silt2	16	3.38	43.67	2.65	7.37
Dow Field Silty Clay		0.91	0.72	1.46	
Limonite		1.80	1.05	1.97	
West Lebanon Gravel		0.64	3.26	0.65	
average value		1.50	1.84	1.82	3.11

Note: The results of Anderson model do not include the two maximum values of Low Plasticity Clay and Silt2.

Conclusion

Based on the freezing characteristics and electrical double-layer of unfrozen water, this study found that the unfrozen water between clay and sand (silt) particle influenced by the coupling of adsorption effects and capillary action and this unfrozen water is called bound-capillary water for short. The bound-capillary water mainly exists in soil with medium and low clay content. The distance of nanopores between the clay particle and sand (or silt) particle is approximately equal to the thickness (≈ 45Å, or 4.5 nm) of the electrical double-layer. The adsorption effects (surface effects) of the clay particles induce the electrical double-layer structure in the bound-capillary water, and the concentration of the bound-capillary water decreases exponentially with distance from the clay surface. The capillary action induces a meniscus shape in the bound-capillary water, and significantly increases the content of the

bound-capillary water.

According to the experimental phenomena, the influence of initial water content on soil freezing characteristic curve (SFCC) can be categorized three types which correspond to the three stages of bound-capillary water with the initial water content. When the initial water content (w_0) ≤ the maximum bound water content (w_{bmax}), the bound-capillary water is mainly affected by adsorption effects, and the content of bound-capillary water varies linearly with the specific surface area. The w_0 slightly affects the measured SFCCs, and the SFCCs with low w_0 are slightly higher than those with high w_0 (Phenomenon 1). Phenomenon 1 and curvature of SFCCs are caused by cation concentration gradient in diffusion-layer. When $w_{bmax} < w_0 <$ maximum water content of the bound-capillary water (w_{bcmax}), increasingly important capillary action induce the meniscus shape in the bound-capillary water, which becomes more obvious closer to the sand surface. The w_0 significantly affects the SFCCs through capillary action. The higher the temperature and initial water content, the greater the discrepancy between SFCCs (Phenomenon 2). When $w_0 > w_{bcmax}$, the shape of the capillary-induced meniscus reaches its maximum curvature, and excess water migrates out of the nanopores. The initial water content only weakly affects the cation concentration gradient distribution, by changing the soil solution concentration (n_0), but does not change the shape of the meniscus of the bound-capillary water. So the SFCCs with low initial water content are situated slightly higher than the SFCCs with high initial water content.

In this study, three fitting equations were established to describe the gradient of the cation concentration in the diffusion-layer. Based on these three fitting equations and the electrical double-layer equation, four theoretical models and a parametric model of unfrozen water were established. The mathematical expressions of the four unfrozen water theoretical models identical the existing 10 semi-empirical models, demonstrating that the bound-capillary water reflects the freezing characteristics of the soils with medium and low clay content. Given the similarity of the expressions between the theoretical models and the semi-empirical models, we consider that the semi-empirical model provides a suitable empirical formula describing the freezing characteristics of the bound-capillary water.

The independent variables of the unfrozen water parametric model are temperature, initial water content and specific surface area. The measured unfrozen water contents of 9 soils verified that the parametric model is suitable for soils with low and medium clay content (clay $\lessapprox$ 24%, $A_S \lessapprox$ 60 m^2/g). In addition, this study provides a simple method for calculating unfrozen water content that relies on only temperature and specific surface area. This simple method provides a convenient way to calculate the unfrozen water content for remote areas with frozen soil but difficult access (such as the Arctic, the Qinghai-Tibet Plateau, and Alaska).

The structure of bound-capillary water is significantly different from that of traditional soil water distribution. Traditional view believed that bound water is located on the surface of clay particles, with capillary water or free water beyond the periphery of the bound water. This study believes that when the soil water content reaches the maximum bound water content and continues to increase, the soil water

will be located on the sand side of the clay-sand (silt) nanopores in the form of meniscus, rather than changing into capillary water or free water in the traditional view. The maximum water content (w_{bcmax}) of bound-capillary water in clay-sand (silt) nanopores is very large. For example, the maximum water content of clay with specific surface area of 60.5 m^2g^{-1} can reach 36.78%. This is also the reason why this study believes that the characteristics of soil freezing are caused by bound-capillary water.

Parameters related to soil salinity and the electrical double-layer in the theoretical models (soil solution concentration n_0, solute valence v, solute ionization number N, diffusion-layer thickness d, shape factors a_1, b_1, a_2, b_2, a_3, b_3) were found here to be constant in non-saline soils. This property significantly simplifies the modeling of unfrozen water, allowing unfrozen water content to be calculated with just the conventional parameters such as specific surface area, temperature, and initial water content. In addition, changes in soil salinity only affect these parameters, and not the mathematical expressions of the unfrozen water models, enabling the same power-law expressions to be applicable for modeling unfrozen water in saline soils.

The values of all parameters except K_f in the unfrozen water theoretical models are calculated from the measured microscopic physical quantities, which shows that the microstructure of the soils has a close relationship with the macroscopic water content. The drawbacks of our study are firstly that the characteristics of bound-capillary water are deduced only from experiments, and secondly that the coupling between adsorption and capillary effects is explained only as a conceptual model based on ion molecular forces. We hope to solve these problems in future research.

Acknowledgments

This research was funded by the Second Tibetan Plateau Scientific Expedition and Research Program, Grant No. 2019QZKK010303. All the experimental data sets are obtained from literature Anderson & Tice (1972), Dobson et al (1985), Xu et al (1985), Wen et al (2012), Ma et al (2015), Chai et al (2018), Tang et al (2018), Zhou et al (2020).

References

Anderson, D. M., & Tice, A. R. (1972). Predicting unfrozen water contents in frozen soils from surface area measurements. *Highway research record, 393*, 12-18.

Anderson, D. M., & Tice, A. R. (1973). The unfrozen interfacial phase in frozen soil water systems. In Physical aspects of soil water and salts in ecosystems. *Springer, Berlin, Heidelberg*, 107-124.

Bai, R., Lai, Y., Zhang, M., Yu, F. (2018).Theory and application of a novel soil freezing characteristic curve. *Applied Thermal Engineering*, 129: 1106-1114. https://doi.org/10.1016/j.applthermaleng.2017.10.121

Bai, R., Lai, Y., You, Z., & Ren, J. (2020). Simulation of heat–water–mechanics process in a freezing soil under stepwise freezing. *Permafrost and Periglacial Processes*, 31(1), 200–212. https://doi.org/10.1002/PPP.2028

Banin, A., & Anderson, D. M. (1974). Effects of salt concentration changes during freezing on the unfrozen water content of porous materials. *Water Resources Research, 10*(1), 124-128. https://doi.org/10.1029/WR010i001p00124

Biskaborn, B. K., Smith, S. L., Noetzli, J., Matthes, H., Vieira, G., Streletskiy, D. A., et al. (2019). Permafrost is warming at a global scale. *Nature Communications*, 10(1), 264–264. https://doi.org/10.1038/S41467-018-08240-4

Boyarskii D.A., Tikhonov V.V., Komarova N.Y. (2002). Model of dielectric constant of bound water in soil for applications of microwave remote sensing. *Progress In Electromagnetics Research*, 35:251-269. https://doi.org/10.2528/PIER01042403

Chai, M., Zhang, J., Zhang, H., Mu, Y., Sun, G., & Yin, Z. (2018). A method for calculating unfrozen water content of silty clay with consideration of freezing point. *Applied Clay Science*, 161, 474-481.https://doi.org/10.1016/j.clay.2018.05.015

Dash, J. G. (1989). Thermomolecular pressure in surface melting: motivation for frost heave. *Science*, *246*(4937), 1591-1593. doi: 10.1126/science.246.4937.1591.

Dash, J. G., Fu, H., & Wettlaufer, J. S. (1995). The premelting of ice and its environmental consequences. *Reports on Progress in Physics*, 58(1), 115–167. https://doi.org/10.1088/0034-4885/58/1/003

Dobson, M. C., Ulaby, F. T., Hallikainen, M. T., & El-Rayes, M. A. (1985). Microwave dielectric behavior of wet soil-Part II: Dielectric mixing models. *IEEE Transactions on Geoscience and Remote Sensing*, (1), 35–46. doi: 10.1109/TGRS.1985.289498

Ge, S., McKenzie, J., Voss, C., & Wu, Q. (2011). Exchange of groundwater and surface-water mediated by permafrost response to seasonal and long term air temperature variation, *Geophysical Research Letters*, 38(14). https://doi:10.1029/2011GL047911.

Hayashi, M. (2013). The Cold Vadose Zone: Hydrological and Ecological Significance of Frozen-Soil Processes. *Vadose Zone Journal*, 12(4), 1–8. https://doi.org/10.2136/VZJ2013.03.0064

Hu, G., Zhao, L., Zhu, X., Wu, X., Wu, T., Li, R., Xie, C., Hao, J. (2020). Review of algorithms and parameterizations to determine unfrozen water content in frozen soil. *Geoderma*, 368, 114277. https://doi.org/10.1016/J.GEODERMA.2020.114277

Iwata, Y., Hayashi, M., Suzuki, S., Hirota, T., & Hasegawa, S. (2010). Effects of snow cover on soil freezing, water movement, and snowmelt infiltration: A paired plot experiment. *Water Resources Research*, 46, W09504. doi:10.1029/2009WR008070

Jin, X., Yang, W., Gao, X., & Li, Z. (2020a). Analysis and Modeling of the Complex Dielectric Constant of Bound Water with Application in Soil Microwave Remote Sensing. *Remote Sensing*, 12(21), 3544. https://doi.org/10.3390/rs12213544

Jin, X., Yang, W., Gao, X., Zhao, J., Li, Z., & Jiang, J. (2020b). Modeling the Unfrozen Water Content of Frozen Soil Based on the Absorption Effects of Clay Surfaces. *Water Resources Research*, 56(12). https://doi.org/10.1029/2020WR027482

Jorgenson, M. T. J. T., Romanovsky, V. R., Harden, J. H., Shur, Y. S., O'Donnell, J. O., Schuur, E. A. G., et al. (2010). Resilience and vulnerability of permafrost to climate change. *Canadian Journal of Forest Research*, 40(7), 1219–1236. 10.1139/X10-060

Konrad, J. M., & McCammon, A. W. (1990). Solute partitioning in freezing soils. *Canadian Geotechnical Journal*, 27(6), 726–736. https://doi.org/10.1139/T90-086

Kurylyk, B. L., Watanabe, K. (2013). The mathematical representation of freezing and thawing processes in variably-saturated, non-deformable soils. *Advances in Water Resources*, 60: 160-177.

https://doi.org/10.1016/j.advwatres.2013.07.016

Li, R., Zhao, L., Wu, T., Wang, Q., Ding, Y., Yao, J., et al. (2019). Soil thermal conductivity and its influencing factors at the Tanggula permafrost region on the Qinghai–Tibet Plateau. *Agricultural and Forest Meteorology*, 264: 235-246.

Ma T., Wei, C., Zhou J., Tian H. (2015). Freezing characteristic curves and water retention characteristics of soils. *Rock and Soil Mechanics*, **37**(1), 192-17. https://doi.org/10.11779/CJGE2015S1033v (in Chinese)

Michalowski, R. L. (1993). A constitutive model of saturated soils for frost heave simulations. *Cold regions science and technology*, *22*(1), 47-63. https://doi.org/10.1016/0165-232X(93)90045-A

Mironov, V.L., Kerr, Y., Wigneron, J.P., Kosolapova, L., Demontoux, F. (2013). Temperature- and Texture-Dependent Dielectric Model for Moist Soils at 1.4 GHz. *IEEE Geoscience and Remote Sensing Letters*, 10(3): 419-423. https://doi.org/10.1109/LGRS.2012.2207878.

Mitchell, J.K., (1992). Fundamentals of Soil Behaviour, 2nd edn. *Wiley*, *New York*, p. 437.

Nicolsky, D. J., Romanovsky, V. E., Panda, S. K., Marchenko, S. S., & Muskett, R. R. (2017). Applicability of the ecosystem type approach to model permafrost dynamics across the Alaska North Slope. *Journal of Geophysical Research*: *Earth Surface*, 122(1), 50-75. https://doi.org/10.1002/2016JF003852

Olphen, H. V. (1964). An introduction to clay colloid chemistry. *Soil Science*, 97(4), 290.

Olphen, H. V. (1977). An introduction to clay colloid chemistry, for clay technologists, geologists, and soil scientists.

Panikov, N., Flanagan, P., Oechel, W., Mastepanov, M., & Christensen, T. (2006). Microbial activity in soils frozen to below −39 °C. *Soil Biology & Biochemistry*, 38(4), 785–794. https://doi.org/10.1016/J.SOILBIO.2005.07.004

Peters, A. (2013). Simple consistent models for water retention and hydraulic conductivity in the complete moisture range. *Water Resources Research*, 49(10): 6765–6780. https://doi.org/10.1002/wrcr.20548

Poutou, E., Krinner, G., Genthon, C., & Noblet-Ducoudré, N. (2004). Role of soil freezing in future boreal climate change. *Climate Dynamics*, *23*(6), 621-639. https://doi.org/10.1007/s00382-004-0459-0

Saarenketo, T. (1998). Electrical properties of water in clay and silty soils. *Journal of applied geophysics*, 40(1-3), 73-88. https://doi.org/10.1016/S0926-9851(98)00017-2

Shang, J. Q., Lo, K. Y., & Quigley, R. M. (1994). Quantitative determination of potential distribution in Stern–Gouy double-layer model. *Canadian Geotechnical Journal*, 31(5), 624-636. https://doi.org/10.1139/t94-075

Tang, L., Wang, K., Jin, L., Yang, G., Jia, H., & Taoum, A. (2018). A resistivity model for testing unfrozen water content of frozen soil. *Cold Regions Science and Technology*, 153, 55-63. https://doi.org/10.1016/j.coldregions.2018.05.003

Tian, H., & Wei, C. (2014). A NMR-based testing and analysis of adsorbed water content. *Scientia Sinica Technologica*, 44(3), 295-305. https://doi.org/10.1360/092013-1133 (in Chinese)

Tripathy S., Sridharan A., Schanz T. (2004). Swelling pressures of compacted bentonites from diffuse double layer theory. *Canadian Geotechnical Journal*, 41(3):437-450. https://doi.org/10.1139/t03-096

Wang, J. R., Schmugge, T.J. (1980) An Empirical Model for the Complex Dielectric Permittivity of Soils as a Function of Water Content. IEEE Transactions on Geoscience and Remote Sensing, GE-18(4): 288-295. https://doi.org/10.1109/TGRS.1980.350304

Walvoord, M.A., & Kurylyk, B.L. (2016). Hydrologic impacts of thawing permafrost—A review, *Vadose Zone Journal*, 15(6), https://doi.org/10.2136/ vzj2016.01.0010

Wang, C., Lai, Y., & Zhang, M. (2017). Estimating soil freezing characteristic curve based on pore-size distribution. *Applied Thermal Engineering*, 124: 1049-1060. https://doi.org/10.1016/j.applthermaleng.2017.06.006

Watanabe, K., Muto, Y., & Mizoguchi, M. (2001). Water and Solute Distributions near an Ice Lens in a Glass-Powder Medium Saturated with Sodium Chloride Solution under Unidirectional Freezing. Crystal Growth & Design, 1(3), 207–211. 10.1021/CG005535I

Watanabe, K., Wake, T. (2009). Measurement of unfrozen water content and relative permittivity of frozen unsaturated soil using NMR and TDR. *Cold Regions Science and Technology*, 59(1): 34-41. https://doi.org/10.1016/j.coldregions.2009.05.011

Wen, Z., Ma, W., Feng, W., Deng, Y., Wang, D., Fan, Z., & Zhou, C. (2012). Experimental study on unfrozen water content and soil matric potential of Qinghai-Tibetan silty clay. *Environmental earth sciences*, 66(5), 1467-1476. https://doi.org/10.1007/s12665-011-1386-0

Xu X. Z, Oliphant J L, Tice A R. (1985). Soil-Water Potential and Unfrozen Water Content and Temperature. Journal of Glaciology and Geocryology, 7(1):1–12. (in Chinese). https://doi.org/CNKI:SUN:BCDT.0.1985-01-000

Xu, X. Z, Wang, J. C, Zhang, L. X., (2010). Frozen Soil Physics Science. *Science Press, Beijing* (in Chinese).

Yang, M., Nelson, F., Shiklomanov, N., Guo, D., & Wan, G. (2010). Permafrost degradation and its environmental effects on the tibetan plateau: a review of recent research. *Earth-Science Reviews*, 103(1–2), 31-44. https://doi.org/10.1016/j.earscirev.2010.07.002

Zhang, C., & Lu, N. (2021). Soil aborptive Potential–Based Paradigm for Soil Freezing Curves. *Journal of Geotechnical and Geoenvironmental Engineering*, 147(9), 4021086. https://doi.org/10.1061/(ASCE)GT.1943-5606.0002597

Zhang, L., Zhuang, Q., Wen, Z., Zhang, P., Ma, W., Wu, Q., & Yun, H. (2021). Spatial state distribution and phase transition of non-uniform water in soils: Implications for engineering and environmental sciences. *Advances in Colloid and Interface Science*, 294, 102465–102465. https://doi.org/10.1016/J.CIS.2021.102465

Zhang, Y., Wang, S., Barr, A.G., Black, T.A. (2008). Impact of snow cover on soil temperature and its simulation in a boreal aspen forest. Cold Regions Science & Technology, 52(3), 355-370. https://doi.org/10.1016/j.coldregions.2007.07.001

Zhou, J., Meng, X., Wei, C., & Pei, W. (2020). Unified soil freezing characteristic for variably saturated and saline soils. *Water Resources Research*, 56(7). https://doi.org/10.1029/2019wr026648

Zhou, J., Wei, C., Lai, Y., Wei, H., & Tian, H. (2018). Application of the Generalized Clapeyron Equation to Freezing Point Depression and Unfrozen Water Content. *Water Resources Research*, 54(11), 9412-9431. https://doi.org/10.1029/2018WR023221